Sound Coding in the Auditory Nerve: From Single Fiber Activity to Cochlear Mass Potentials in Gerbils

A. Huet, C. Batrel, J. Wang, G. Desmadryl, Regis Nouvian, J.L. Puel, J. Bourien

Sound coding in the auditory nerve: from single fiber activity to cochlear mass potentials in gerbils

Huet A., Batrel C., Wang J., Desmadryl G., Nouvian R., Puel J.L.,[~§] and Bourien J.[~]

INM, Inserm, Univ Montpellier, Montpellier, France

Authorship note: ~ : These authors contributed equally

[§] : **Corresponding author**:

Jean-Luc PUEL: INM-INSERM U 1051, 80 rue Augustin Fliche, 34295 Montpellier, France,

Tel: (+33) 499 636 009, Fax: (+33) 499 636 020, e-mail: jean-luc.puel@inserm.fr.

Acknowledgments and Funding sources: This work was supported by Institut National de la Santé et de la Recherche Médicale Grant U10512F/U1051SE12FE, the Inserm Grant (U1051-Dot 02-2015), Fondation de l'Avenir Project Et2-675, Cochlear France Award (R11055FF/RVF11006FFA), Agence Nationale pour la Recherche (ANR-13-JSV1-0009-01) and "Prix Scientifique" from "Fondation pour l'Audition". The authors acknowledge language services (www.stels-ol.de) for editing assistance.

Keywords: Temporal coding, rate coding, auditory nerve, background noise, hidden hearing loss

ABSTRACT

Auditory nerve fibers (ANFs) convey acoustic information from the sensory cells to the brainstem using an elaborated neural code based on both spike timing and rate. As the stimulus tone frequency increases, time coding fades and ceases, resulting in high-frequency tone encoding relies mostly on the spike discharge rate. Here, we recapitulated our recent single unit data from gerbil's auditory nerve to highlight the most relevant mode of coding (spike timing *versus* spike rate) in tone-in-noise. We report that high-spontaneous rate (SR) fibers driven by low-frequency tones in noise are able to phase lock ~30 dB below the level that evoked a significant elevation of the discharge rate, whereas medium- and low-SR fibers switch their preferential mode of coding from rate coding in quiet, to time coding in noise. For high-frequency tone, the low-threshold/high-SR fibers reach their maximum discharge rate in noise and do not respond to tones, whereas medium- and low-SR fibers are still able to respond to tones making them more resistant to background noise. Based on these findings, we first discuss the ecological function of the ANF distribution according to their spontaneous discharge rate. Then, we point out the poor synchronization of the low-SR ANFs, accounting for the discrepancy between ANF number and the amplitude of the compound action potential of the of the auditory nerve. Finally, we proposed a new diagnostic tool to assess low-SR fibers, which does not rely on the onset response of the ANFs.

Highlights:

- Functional properties of ANFs were examined in quiet and noisy backgrounds.
- In low-frequency range, high-SR fibers use temporal coding to encode tone in noise.
- In high-frequency range, low-SR fibers encode tone-in-noise using rate coding.
- Low-SR fibers are not detectable using the CAP of the auditory nerve.
- Round-window mass potentials enable assessment of low-SR fibers.

INTRODUCTION

Auditory nerve fibers (ANFs) are the functional units that transmit the neural message from the cochlea toward the cochlear *nuclei*. The pioneering study of Liberman (1978) in the cat demonstrated that 3 classes of fibers populate the auditory nerve when classified according to their spontaneous rate (SR): the high- ($\geq$ 18 spikes/s), the medium- (0.5 $\leq$ SR < 18 spikes/s) and the low- (< 0.5 spike/s) SR fibers. While high- and medium-SR fibres are activated in response to lower sound pressure levels but rapidly saturate, low-SR fibres are recruited at higher sound pressure levels and show little or no saturation (Winter et al., 1990). This large scatter of behaviours makes the ANFs capable of encoding sounds over a large intensity range (Taberner and Liberman, 2005). Tone frequencies also determine the patterns of action potential discharge of the ANFs. In response to low-frequency tones, ANF firing is phase locked to the sinusoidal waveform, *i.e.* action potentials are fired at a preferential phase of the periodic stimulation (Rose et al., 1967; Anderson et al., 1971; Johnson, 1980). As the frequency increases, this time-coding ability decreases and the encoding of high-frequency tones relies on the place of the maximum excitation on the cochlea, leading to changes in the rate of firing (rate-place code). In other words, high-frequency tone is encoded through a rate-place code whereas the coding of low-frequency tones relies on both spike timing and rate-place codes.

In the presence of background noise, masking produces a compression and a shift of the rate-intensity function toward higher tone levels (Costalupes et al., 1984). Increasing the noise level leads to a flat rate-intensity function, with no detectable increment of discharge rate to tones in noise. Because this phenomenon preferentially affects the low-threshold/high-SR ANFs, low-SR fibers coding for higher levels were originally thought to be more resistant to background noise. However, this theory is only based on the discharge rate of the auditory

nerve fibers. In the low-frequency range, phase-locked responses to low-level tones decrease with increasing masker level, but phase locking remains quite strong near behavioral masking thresholds (Abbas, 1981; Costalupes, 1985). Studies in humans consistently report that tone detection in noise might be partly determined by synchrony to the fine structure of the tone (Moore and Raab, 1975; Moore, 2003; Zeng et al., 2005; Lorenzi et al., 2006; Vinay and Moore, 2007; Kortlang et al., 2016). It thus seems that both spike timing and spike rate are involved in tone-in-noise detection.

The aim of the present review is to recapitulate our recent data from gerbils auditory nerve activity to highlight : *i*) how time and rate encoding modes operate in quiet and noisy environments, *ii*) how the ANF distribution matches the ecological environment, and *iii*) why cochlear mass potential recorded from the round window may be a better proxy of the SR-based distribution of ANFs than the regular auditory brainstem responses (ABRs) used for experimental and clinical evaluation of hearing.

1. Sound encoding in the auditory nerve

After being mechanically amplified by the outer hair cells (OHCs), the vibration of the basilar membrane is converted into trains of action potentials by the IHCs and conveyed along ANFs to the cochlear *nuclei*. The characteristic frequency (CF) of an ANF is the frequency for which a minimal amount of energy is required to increase the discharge rate above the SR. SR and threshold are negatively correlated, *i.e.*, fibers of high-SR have lower thresholds and *vice versa* (see for review Heil and Peterson, 2015).

1.1. Tone encoding in quiet

The methods for recording single fibers of auditory nerve in gerbils have been extensively described in Bourien et al. (2014). Briefly, the surgical approach to the auditory nerve was through the posterior fossa after a craniotomy (**Figure 1**). Single units (n = 377 fibers) from the auditory nerve were recorded in 44 adults gerbils (2 to 6 month-old). Once a fiber was isolated, its CF and threshold values were determined from the tip of the tuning curve, and the SR was calculated over a 30s sample. In **Figure 2**, the tone-evoked receptor potential of the IHCs (**Figure 2A**, adapted from Palmer and Russell, 1986) is compared with the peristimulus-time histograms (PSTHs) constructed from spike timing when driven by repetitive acoustic stimulation **(Figure 2B**). To do so, we used the same acoustic parameters as Palmer and Russel in 1986 (*i.e.* 50 ms tone bursts, 1 ms rise and fall, 10 bursts/s). Akin to the IHC receptor potentials, the ANF responses were phase-locked to the tone: *i.e.* they fired action potentials at a preferred phase of the sinewave (**Figure 2B**). Such phase locking to the fine structure in response to low-frequency pure tones occurs up to few kilohertz, depending on the species; up to 4-5 kHz in cats (Kiang et al., 1965) and gerbils (Versteegh et al., 2011), 3–4 kHz in guinea pigs (Palmer and Russell, 1986) and chinchillas (Temchin and Ruggero, 2010), around 4 kHz in mice (Taberner and Liberman, 2005), and 3 kHz in ferrets (Sumner and Palmer, 2012). These limits correspond to the maximum frequency that can be encoded by the alternating current (AC) membrane-potential fluctuations in IHCs (**Figure 2A, B**). The IHC acts as a low-pass filter, as its membrane potential cannot follow fast fluctuations due to the membrane time constant. The IHC attenuates the AC component of the IHC response until, at a sufficiently high frequency depending of the species only a direct current (DC) component remains (Palmer and Russell, 1986). To quantify the degree of spike coincidence across the presentations of the stimulus as a proxy for temporal coding, Huet et al. (2018) computed shuffled autocorrelograms to obtain the correlation index (CI, Joris et al., 2006). For the low-CF ANFs, the shuffled autocorrelogram (SAC) is characterized by a large central peak and

multiple adjacent oscillations, attesting to strong neural phase locking to the fine structure of the tone burst (**Figure 2C, D**). For the high-CF ANFs, the peak height of the SAC and of adjacent oscillations were strongly reduced, indicating that neural phase locking was failing (**Figure 2D**). In others words, the remaining central peak mostly reflected the small temporal jitter of the first spike at the tone-burst onset. Based on this index, the limit of phase locking in gerbil approximated 4 kHz **(Figure 2D)**.

Another characteristic of the sound-evoked ANF response is the rapid decrease of the spiking rate within the first ten milliseconds after the onset of the tone burst to a steady state (**Figure 2B**). This adaptive response arises most probably from the reduction in the number of synaptic vesicles in the vicinity of the calcium channels, *i.e*. the readily releasable pool. While readily releasable vesicles mediate the high rate at the stimulus onset, the lower, steady-state response reflects the vesicular re-supply at the release sites (Furukawa and Matsuura, 1978; Moser and Beutner, 2000; Spassova et al., 2004).

1.2. Tone encoding in noise

To clearly separate time and rate modes, Huet et al. (2018) used a simple paradigm of acoustic stimulation that used tone-burst sequences embedded in continuous 60 dB SPL pink noise. The additional energy supplied by adding noise produced an increase in the low-level discharge rate, a threshold shift to the higher levels, and a decrease in the maximum discharge rate, which could lead to a flat rate-intensity function (**Figure 3A1-F1**). Among the 377 fibers recorded by Huet et al. (2018), 175 (46%) reached their maximum discharge rate in noise, making difficult to estimate a threshold, and hence, the threshold therefore referred to the higher level tested, *i.e*. 80 dB SPL (see for example **Figure 3A$_1$**). Taking advantage of the correlation index (CI, Joris et al., 2006) as a unique proxy, we presently quantified the spike synchrony across multiple presentations of the tone for all the fibers (**Figure 3A$_2$-F$_2$**). In the

range of the neural phase locking, CI showed a large and step-wise elevation with increasing sound intensity, followed by a slow decline (Insert **Figure 2D**, **Figure 3A$_2$-C$_2$**). For higher frequencies, the CI grew linearly with sound intensity, but remained at a small amplitude (just above 1), because it reflects the precision of the first spike latency at the onset of the tone-burst envelope (**Figure 3D$_2$-F$_2$**).

To facilitate the comparison between the two modes of coding (*i.e.* time *versus* rate), we plot CI as a function of the level relative to the rate threshold (**Figure 4A-F**), as proposed by Dreyer and Delgutte (2006). This figure emphasizes the preferential coding mode in tone-in-noise. When the CI-based threshold was shifted to lower or to higher intensities-with respect to the rate threshold, the threshold favors time or rate encoding, respectively. We separated the low-CF (**Figure 4A-C**) and the high-CF ANFs (**Figure 4D-F)** according to the cut-off frequency between the two modes of coding calculated by Huet et al., (2018), corresponding to 2.7 kHz. Moreover, we divided the 377 fibers according to the classification proposed by Liberman (1978) in the cat : *i.e.*, high- ($\geq$ 18 spikes/s), medium- (0.5 $\leq$ SR < 18 spikes/s) and the low-SR fibers (< 0.5 spike/s). In the range of phase locking (**Figure 4A-C)**, the high-SR fibers, which constitute 31% of the whole contingent of fibers in gerbils, were clearly more adapted than low-SR fibers, to detect low-frequency tones (6 dB below rate threshold in quiet). The same high-SR pool of ANFs in the presence of background noise continued to respond in time rather than in rate. Moreover, high-SR fibers in noise were able to phase lock 30 dB below the level that induced a detectable elevation of their discharge rate (**Figure 4A**). Another interesting finding is the switch of the coding mode from a rate code in quiet, to a time code in noise for the medium- and the low-SR, which represent 9% of fibers (**Figure 4B, C).** This most likely occurred because the noise evoked enough spikes in these fibers to elicit a phase-locked response. For the high-frequency range, all the fibers responded with a

rate code and the temporal coding only rely on the temporal precision of the first spike triggered at the tone burst onset (**Figure 4D-F**).

To summarize, the high-SR ANFs are more adapted to carry neural information through a spike-timing mode, giving them a strong robustness to detect low-frequency tones in background noise. In the high-frequency range, low-threshold/high-SR fibers reach their maximum discharge in noise, making them inefficient to respond to tones, and only the low- and medium SR that have a more elevated thresholds can encode tone in noise. Interestingly, Huet et al. (2018) reported that the time-based sensitivity of ANFs nicely overlaps with the low-frequency behavioral audiogram evaluated through prepulse inhibition of the acoustical startle responses up to 4 kHz, whereas the rate-based threshold fitted the behavioral thresholds above 4 kHz.

1.3. Ecological function of different types of fibers

A distinction into three pools of ANFs based on SR has been described in cats (Liberman, 1978), guinea pigs (Tsuji and Liberman, 1997), and gerbils (Schmiedt, 1989), yet the respective distribution across the cochlear tonotopic axis differs between species. For example, cochleae from guinea pigs shows a regular distribution of high- (75%), medium- (15%) and low-SR (10%) fibers along the tonotopic axis (Tsuji and Liberman, 1997). In the gerbil, the distribution of the fibers along the base to apex gradient is heterogeneous. Pooling all the fibers in gerbils (n = 1005 fibers, Huet et al., 2016) shows a heterogeneous distribution of ANFs from base to apex, resulting in two different auditory-nerve phenotypes across the tonotopic gradient (**Figure 5A**). We then quantified the proportion of the ANFs below and above the cut-off frequency between the two modes of coding calculated by Huet et al. (2018). High-SR fibers represent 29% and 25%, medium-SR fibers represent 6% and 27%,

and low-SR fibers represent 3% and 14%, for fiber CF below and above 2.7 kHz, respectively (**Figure 5A**). Note that these proportions are quite similar to those found in a smallest sample of fibers (n = 377 fibers), in which we have investigated the time *versus* rate of coding in response to tone-in-noise (see **Figure 4**).

One intriguing question is why the distribution into three pools of fibers (high-, medium- and low-SR) across the tonotopic axis differs between species. One hypothesis is that the different pools of ANFs reflect the benefits arising from ecological functions. Plotting the cumulative number of fibers per octave band shows a clear bimodal distribution with a majority of high-SR ANFs below 4 kHz and a more balanced distribution above (**Figure 5B**). This greater proportion of high-SR fibers in the low-frequency range may reflect the need to detect and localize the rhythmic thumping sound that their conspecifics make with their hind feet to warn of the presence of predators (*e.g.* a hunting owl). Indeed, the foot-stamping produces a low-frequency sound around 1 kHz (Lay, 1972; Müller, 1996). In addition, gerbils exhibited a rich repertoire of vocalizations with fundamental frequencies of 5 to 50 kHz (Kobayasi and Riquimaroux, 2012). Consequently, the more balanced distribution above 4 kHz would enable the vocalizations to operate over large dynamic ranges through high-, medium- and low-SR fibers. Thus, the predominance of high-SR fibers below 4 kHz (**Figure 5A, B**), and the greater proportion of low-SR ANFs in the higher-frequency range may help gerbils to communicate in noisy environments.

2. Toward a new diagnostic test to map the auditory nerve

Sound-evoked compound action potential (CAP) of the auditory nerve, which captures the synchronous activation of the auditory nerve fibers, is commonly used to diagnose deafness in experimental and clinical settings. It is generally believed that all the ANFs contribute to the

CAP threshold and amplitude: low sound-pressure levels activate the high-SR fibers, and increasing levels gradually recruit medium- and then low-SR ANFs. However, Schuknecht first pointed out that the classical tonal audiogram shows very little change until neural loss exceeds 80-90% (Schuknecht and Woellner, 1955). The same conclusion was drawn for the electrophysiological thresholds evaluated from the wave I of ABRs, or from the auditory-nerve CAP recorded at the round window (Liberman and Kujawa, 2017). This phenomenon, called "hidden hearing loss," has been described in various type of cochlear diseases such as noise trauma (Kujawa and Liberman, 2009; Lin et al., 2011; Liberman and Kujawa, 2017), ototoxic drugs (Bourien et al., 2014; Lobarinas et al., 2016), and aging (Menardo et al., 2012; Sergeyenko et al., 2013).

It is well known that ANF can be destroyed by infusing ouabain into the round window niche (Schmiedt et al., 2002). We already showed (Bourien et al., 2014) that infusion of 33 µM ouabain into the round window niche for 30 minutes led, 6 days after the application, to the ablation of 11 % of the fibers coding the 16 kHz region (**Figure 6 A-C**), corresponding to the low-SR fibers (**Figure 6 D-E**). There was no accompanying change in CAP threshold or amplitude **(Figure 6F**). Increasing the ouabain concentration up to 66 µM led to 65% low- and medium-SR ANFs loss with no change in threshold, but a substantial decrease in CAP amplitude (~50% amplitude reduction, **Figure 6 G-I**). Based on single fiber recordings in the auditory nerve, we showed that first-spike latency of the low-SR fibers was delayed and broadly dispersed in response to tone bursts (Bourien et al., 2014). Thus, the loss of 16 % of poorly synchronized, low-SR ANFs at 16 kHz and responding to the higher level did not alter the CAP amplitude. In contrast, the smaller size in the CAP amplitude following the 65% ANF loss may reflect the loss of fibers showing a synchronized onset response (medium-SR

fibers). Finally, only 34% of high-SR fibers, which show a large synchronized activity at low levels of sound stimulation, sufficed to obtain a “normal” CAP threshold.

The mechanisms underlying the different synchronization properties of the low- and high-SR ANFs are unknown. They may arise from different degrees of coordination in synaptic release at the IHC ribbon synapse (Beutner et al., 2001; Frank et al., 2009; Meyer et al., 2009; Grant et al., 2010) and/or different properties at the spike initiation site near the *habenula perforata* (Siegel, 1992; Hossain et al., 2005; Rutherford et al., 2012; Kim and Lim, 2016). Alternatively, the inhibitory effect of dopamine from the lateral olivocochlear efferent bundle may constitute an additional mechanism that sets the intrinsic properties of the ANFs (Ruel et al., 2001).

To circumvent the synchronization issue, we developed a new protocol of acoustic stimulation and signal processing based on the electrical neural noise recorded at the round window (Batrel et al., 2017). The hallmark of this electrical neural noise (also call mass potential) corresponds to a spectral component that is best described by a power spectrum density with a predominant peak near 900 Hz (**Figure 7A**). In response to sound stimulation, the mass potential contains both a neural component arising from ANFs, and a microphonic component originating from transduction currents in hair cells (Dallos, 1973). To eliminate the microphonic component, we used repetitive pairs of sounds of opposite polarities, and the neural index was calculated by dividing point-by-point the response to sound by values for the unstimulated condition (**Figure 7B, C**). Note that the bimodal shape of the amplitude of the neural index matches with the cumulative number of high-, medium- and low-SR along the tonotopic axis (compare **Figure 5B and Figure 7D**). Figure 7E shown that ouabain-induced deletion of low-SR fibers leads to a reduction in the high-frequency response (where the low-SR fibers are preferentially located, see **Figure 5B, Figure 6 C-E**), while the amplitude of CAP of the auditory nerve did not change (**Figure 6F**).

In conclusion, growing evidence suggests that ANF loss may contribute to problems of speech comprehension in difficult listening environments (Liberman et al., 2016), and may be responsible for the generation of tinnitus and/or hyperacusis (see Knipper et al., 2013 for a review). Consequently, mass potentials that track all the ANFs may constitute a promising avenue to probe ANF loss in humans. However, these potentials are poorly defined using far-field electrodes because of the very low signal amplitudes. The need for near-field electrodes directly placed on the cochlear nerve during cerebellopontine angle surgery, or the placement of a trans-tympanic electrode on the promontory near the round window through the anesthetized tympanic membrane may be an option, but with serious limits as a diagnostic tool. Another solution may come from the use of a noninvasive ball electrode directly apposed to the tympanic membrane in the external auditory canal, which allowed a significantly greater signal amplitude than wave I of the ABR (Roland et al., 1995; Schoonhoven et al., 1995; Pappas et al., 2000; Krieg et al., 2014; Pardo-Jadue et al., 2017). Further experiments in animals and humans need to be carried out before considering mass potentials as a potential diagnostic tool.

References :

Abbas PJ (1981) Auditory-nerve fiber responses to tones in a noise masker. Hear Res 5:69–80.

Anderson DJ, Rose JE, Hind JE, Brugge JF (1971) Temporal position of discharges in single auditory nerve fibers within the cycle of a sine-wave stimulus: frequency and intensity effects. J Acoust Soc Am 49:Suppl 2:1131+.

Batrel C, Huet A, Hasselmann F, Wang J, Desmadryl G, Nouvian R, Puel J-L, Bourien J (2017) Mass Potentials Recorded at the Round Window Enable the Detection of Low Spontaneous Rate Fibers in Gerbil Auditory Nerve. PLoS ONE 12:e0169890.

Beutner D, Voets T, Neher E, Moser T (2001) Calcium dependence of exocytosis and endocytosis at the cochlear inner hair cell afferent synapse. Neuron 29:681–690.

Bourien J, Tang Y, Batrel C, Huet A, Lenoir M, Ladrech S, Desmadryl G, Nouvian R, Puel J-L, Wang J (2014) Contribution of auditory nerve fibers to compound action potential of the auditory nerve. J Neurophysiol 112:1025–1039.

Costalupes JA (1985) Representation of tones in noise in the responses of auditory nerve fibers in cats. I. Comparison with detection thresholds. J Neurosci 5:3261–3269.

Costalupes JA, Young ED, Gibson DJ (1984) Effects of continuous noise backgrounds on rate response of auditory nerve fibers in cat. J Neurophysiol 51:1326–1344.

Dallos P (1973) The Auditory Periphery. Biophysics and Physiology. Available at: https://www.scholars.northwestern.edu/en/publications/the-auditory-periphery-biophysics-and-physiology [Accessed June 26, 2018].

Dreyer A, Delgutte B (2006) Phase locking of auditory-nerve fibers to the envelopes of high-frequency sounds: implications for sound localization. J Neurophysiol 96:2327–2341.

Frank T, Khimich D, Neef A, Moser T (2009) Mechanisms contributing to synaptic Ca2+ signals and their heterogeneity in hair cells. Proc Natl Acad Sci USA 106:4483–4488.

Furukawa T, Matsuura S (1978) Adaptive rundown of excitatory post-synaptic potentials at synapses between hair cells and eight nerve fibres in the goldfish. J Physiol (Lond) 276:193–209.

Grant L, Yi E, Glowatzki E (2010) Two modes of release shape the postsynaptic response at the inner hair cell ribbon synapse. J Neurosci 30:4210–4220.

Heil P, Peterson AJ (2015) Basic response properties of auditory nerve fibers: a review. Cell Tissue Res 361:129–158.

Hossain WA, Antic SD, Yang Y, Rasband MN, Morest DK (2005) Where is the spike generator of the cochlear nerve? Voltage-gated sodium channels in the mouse cochlea. J Neurosci 25:6857–6868.

Huet A, Batrel C, Tang Y, Desmadryl G, Wang J, Puel J-L, Bourien J (2016) Sound coding in the auditory nerve of gerbils. Hear Res. 338:32-9.

Huet A, Desmadryl G, Justal T, Nouvian R, Puel J-L, Bourien J (2018) The Interplay Between Spike-Time and Spike-Rate Modes in the Auditory Nerve Encodes Tone-In-Noise Threshold. J Neurosci 38:5727–5738.

Johnson DH (1980) The relationship between spike rate and synchrony in responses of auditory-nerve fibers to single tones. J Acoust Soc Am 68:1115–1122.

Joris PX, Louage DH, Cardoen L, van der Heijden M (2006) Correlation index: a new metric to quantify temporal coding. Hear Res 216–217:19–30.

Kiang NY, Watanabe T, Thomas EC, Clark LF (1965) Discharge Patterns of Single Fibers in the Cat's Auditory Nerve. In. Cambridge, Massachusetts: The MIT Press.

Kim S-Y, Lim W (2016) Effect of network architecture on burst and spike synchronization in a scale-free network of bursting neurons. Neural Netw 79:53–77.

Knipper M, Van Dijk P, Nunes I, Rüttiger L, Zimmermann U (2013) Advances in the neurobiology of hearing disorders: recent developments regarding the basis of tinnitus and hyperacusis. Prog Neurobiol 111:17–33.

Kobayasi KI, Riquimaroux H (2012) Classification of vocalizations in the Mongolian gerbil, Meriones unguiculatus. J Acoust Soc Am 131:1622–1631.

Kortlang S, Mauermann M, Ewert SD (2016) Suprathreshold auditory processing deficits in noise: Effects of hearing loss and age. Hear Res 331:27–40.

Krieg SM, Kempf L, Droese D, Rosahl SK, Meyer B, Lehmberg J (2014) Superiority of tympanic ball electrodes over mastoid needle electrodes for intraoperative monitoring of hearing function. J Neurosurg 120:1042–1047.

Kujawa SG, Liberman MC (2009) Adding insult to injury: cochlear nerve degeneration after "temporary" noise-induced hearing loss. J Neurosci 29:14077–14085.

Lay DM (1972) The anatomy, physiology, functional significance and evolution of specialized hearing organs of gerbilline rodents. J Morphol 138:41–120.

Liberman MC (1978) Auditory-nerve response from cats raised in a low-noise chamber. J Acoust Soc Am 63:442–455.

Liberman MC, Epstein MJ, Cleveland SS, Wang H, Maison SF (2016) Toward a Differential Diagnosis of Hidden Hearing Loss in Humans. PLoS ONE 11:e0162726.

Liberman MC, Kujawa SG (2017) Cochlear synaptopathy in acquired sensorineural hearing loss: Manifestations and mechanisms. Hear Res 349:138–147.

Lin HW, Furman AC, Kujawa SG, Liberman MC (2011) Primary neural degeneration in the Guinea pig cochlea after reversible noise-induced threshold shift. J Assoc Res Otolaryngol 12:605–616.

Lobarinas E, Salvi R, Ding D (2016) Selective Inner Hair Cell Dysfunction in Chinchillas Impairs Hearing-in-Noise in the Absence of Outer Hair Cell Loss. J Assoc Res Otolaryngol 17:89–101.

Lorenzi C, Gilbert G, Carn H, Garnier S, Moore BCJ (2006) Speech perception problems of the hearing impaired reflect inability to use temporal fine structure. Proc Natl Acad Sci USA 103:18866–18869.

Menardo J, Tang Y, Ladrech S, Lenoir M, Casas F, Michel C, Bourien J, Ruel J, Rebillard G, Maurice T, Puel J-L, Wang J (2012) Oxidative stress, inflammation, and autophagic stress as the key

mechanisms of premature age-related hearing loss in SAMP8 mouse Cochlea. Antioxid Redox Signal 16:263–274.

Meyer AC, Frank T, Khimich D, Hoch G, Riedel D, Chapochnikov NM, Yarin YM, Harke B, Hell SW, Egner A, Moser T (2009) Tuning of synapse number, structure and function in the cochlea. Nat Neurosci 12:444–453.

Moore BC, Raab DH (1975) Intensity discrimination for noise bursts in the presence of a continuous, bandstop background: effects of level, width of the bandstop, and duration. J Acoust Soc Am 57:400–405.

Moore BCJ (2003) An Introduction to the Psychology of Hearing, 5th Revised edition. Amsterdam ; Boston: Academic Press Inc.

Moser T, Beutner D (2000) Kinetics of exocytosis and endocytosis at the cochlear inner hair cell afferent synapse of the mouse. Proc Natl Acad Sci USA 97:883–888.

Müller M (1996) The cochlear place-frequency map of the adult and developing Mongolian gerbil. Hear Res 94:148–156.

Palmer AR, Russell IJ (1986) Phase-locking in the cochlear nerve of the guinea-pig and its relation to the receptor potential of inner hair-cells. Hear Res 24:1–15.

Pappas DG, Pappas DG, Carmichael L, Hyatt DP, Toohey LM (2000) Extratympanic electrocochleography: diagnostic and predictive value. Am J Otol 21:81–87.

Pardo-Jadue J, Dragicevic CD, Bowen M, Delano PH (2017) On the Origin of the 1,000 Hz Peak in the Spectrum of the Human Tympanic Electrical Noise. Front Neurosci 11:395.

Roland PS, Yellin MW, Meyerhoff WL, Frank T (1995) Simultaneous comparison between transtympanic and extratympanic electrocochleography. Am J Otol 16:444–450.

Rose JE, Brugge JF, Anderson DJ, Hind JE (1967) Phase-locked response to low-frequency tones in single auditory nerve fibers of the squirrel monkey. J Neurophysiol 30:769–793.

Ruel J, Nouvian R, Gervais d'Aldin C, Pujol R, Eybalin M, Puel JL (2001) Dopamine inhibition of auditory nerve activity in the adult mammalian cochlea. Eur J Neurosci 14:977–986.

Rutherford MA, Chapochnikov NM, Moser T (2012) Spike encoding of neurotransmitter release timing by spiral ganglion neurons of the cochlea. J Neurosci 32:4773–4789.

Ryan A (1976) Hearing sensitivity of the mongolian gerbil, Meriones unguiculatis. J Acoust Soc Am 59:1222–1226.

Schmiedt RA (1989) Spontaneous rates, thresholds and tuning of auditory-nerve fibers in the gerbil: comparisons to cat data. Hear Res 42:23–35.

Schmiedt RA, Okamura H-O, Lang H, Schulte BA (2002) Ouabain application to the round window of the gerbil cochlea: a model of auditory neuropathy and apoptosis. J Assoc Res Otolaryngol 3:223–233.

Schoonhoven R, Fabius MA, Grote JJ (1995) Input/output curves to tone bursts and clicks in extratympanic and transtympanic electrocochleography. Ear Hear 16:619–630.

Schuknecht HF, Woellner RC (1955) An experimental and clinical study of deafness from lesions of the cochlear nerve. J Laryngol Otol 69:75–97.

Sergeyenko Y, Lall K, Liberman MC, Kujawa SG (2013) Age-related cochlear synaptopathy: an early-onset contributor to auditory functional decline. J Neurosci 33:13686–13694.

Siegel JH (1992) Spontaneous synaptic potentials from afferent terminals in the guinea pig cochlea. Hear Res 59:85–92.

Spassova MA, Avissar M, Furman AC, Crumling MA, Saunders JC, Parsons TD (2004) Evidence that rapid vesicle replenishment of the synaptic ribbon mediates recovery from short-term adaptation at the hair cell afferent synapse. J Assoc Res Otolaryngol 5:376–390.

Sumner CJ, Palmer AR (2012) Auditory nerve fibre responses in the ferret. Eur J Neurosci 36:2428–2439.

Taberner AM, Liberman MC (2005) Response properties of single auditory nerve fibers in the mouse. J Neurophysiol 93:557–569.

Temchin AN, Ruggero MA (2010) Phase-locked responses to tones of chinchilla auditory nerve fibers: implications for apical cochlear mechanics. J Assoc Res Otolaryngol 11:297–318.

Tsuji J, Liberman MC (1997) Intracellular labeling of auditory nerve fibers in guinea pig: central and peripheral projections. J Comp Neurol 381:188–202.

Versteegh CPC, Meenderink SWF, van der Heijden M (2011) Response characteristics in the apex of the gerbil cochlea studied through auditory nerve recordings. J Assoc Res Otolaryngol 12:301–316.

Vinay null, Moore BCJ (2007) Ten(HL)-test results and psychophysical tuning curves for subjects with auditory neuropathy. Int J Audiol 46:39–46.

Winter IM, Robertson D, Yates GK (1990) Diversity of characteristic frequency rate-intensity functions in guinea pig auditory nerve fibres. Hear Res 45:191–202.

Zeng F-G, Kong Y-Y, Michalewski HJ, Starr A (2005) Perceptual consequences of disrupted auditory nerve activity. J Neurophysiol 93:3050–3063.

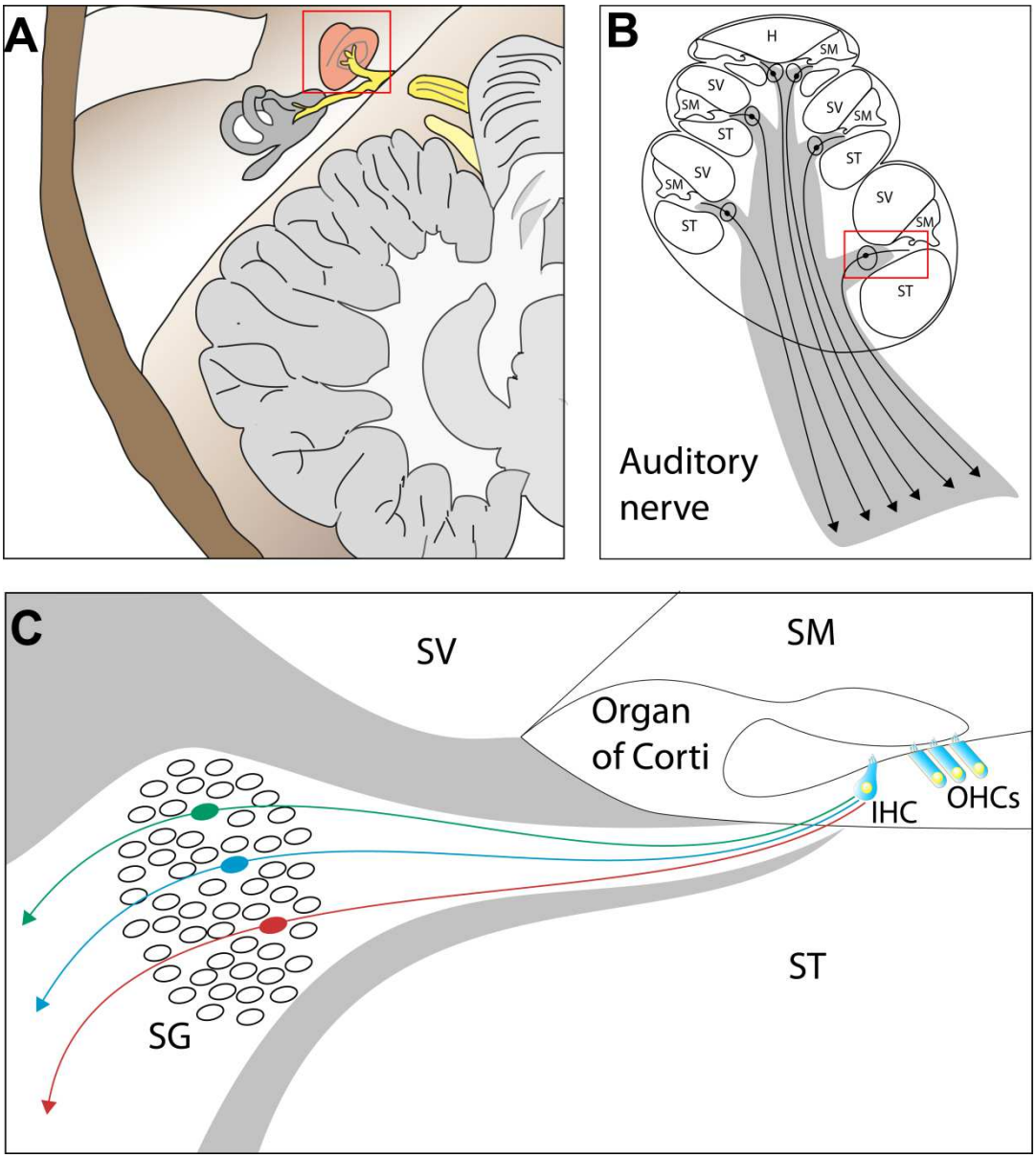

Figure 1: Schematic draw of the cochlea and the auditory nerve. A. Shown is the surgical approach to access the auditory nerve after removing the cerebellum and slightly pushing the brainstem. **B**. Magnification of the cochlea and the auditory nerve from the red square seen in A. Note the cochlea is made up of three canals wrapped around a bony axis, the modiolus. These canals are the scala tympani (ST), the scala vestibuli (SV) and the scala media (SM). **C**. Transverse section of one cochlear turn. The organ of Corti is composed of one row of inner hair cells (IHC) and three rows of outer hair cells (OHCs). The spiral ganglion (SG) is composed of cell bodies of the primary auditory neurons.

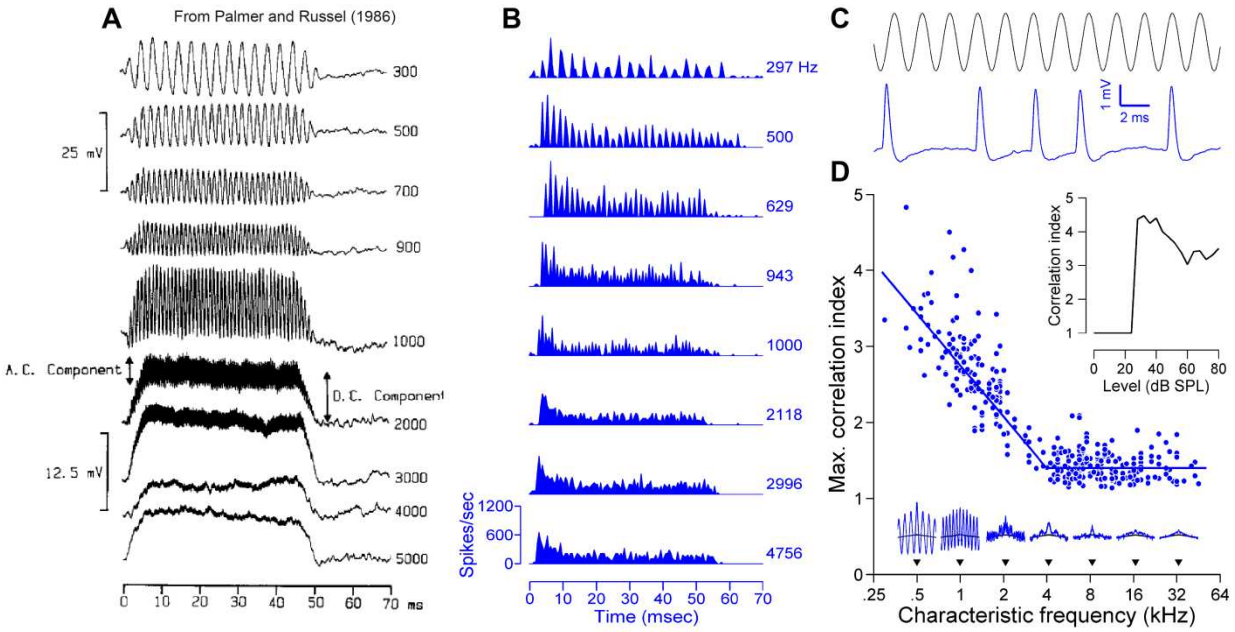

Figure 2: Neural phase locking in the auditory nerve fibers. **A.** Intracellular receptor potentials recorded from a guinea pig IHC in response to 80 dB SPL tones at frequencies indicated in Hertz on the right side of each trace (adapted from Palmer and Russell, (1986), Figure 9). **B**. Peristimulus time histograms recorded from gerbil ANFs in response to 80 dB SPL tones at CF indicated in Hertz on the right side of each trace. **C.** Phase-locked response of a low-CF fiber stimulated with a pure tone presented at CF=530 Hz and 80 dB SPL. **D**. Phase locking as a function of the fiber CF, quantified with the maximum correlation index (CI). *Insets on the top right*: Example of CI *versus* intensity function for a low-CF fiber (CF=900 Hz). *Insets on the bottom*: Examples of normalized shuffle autocorrelograms for fibers with CF indicated by triangles along the *x*-axis. Fit is a broken-stick model ($f(x)$=max(-2.25x + 9.5; 1.4) with x=log(CF), $r^2 \geq 0.78$, cutoff at 4 kHz).

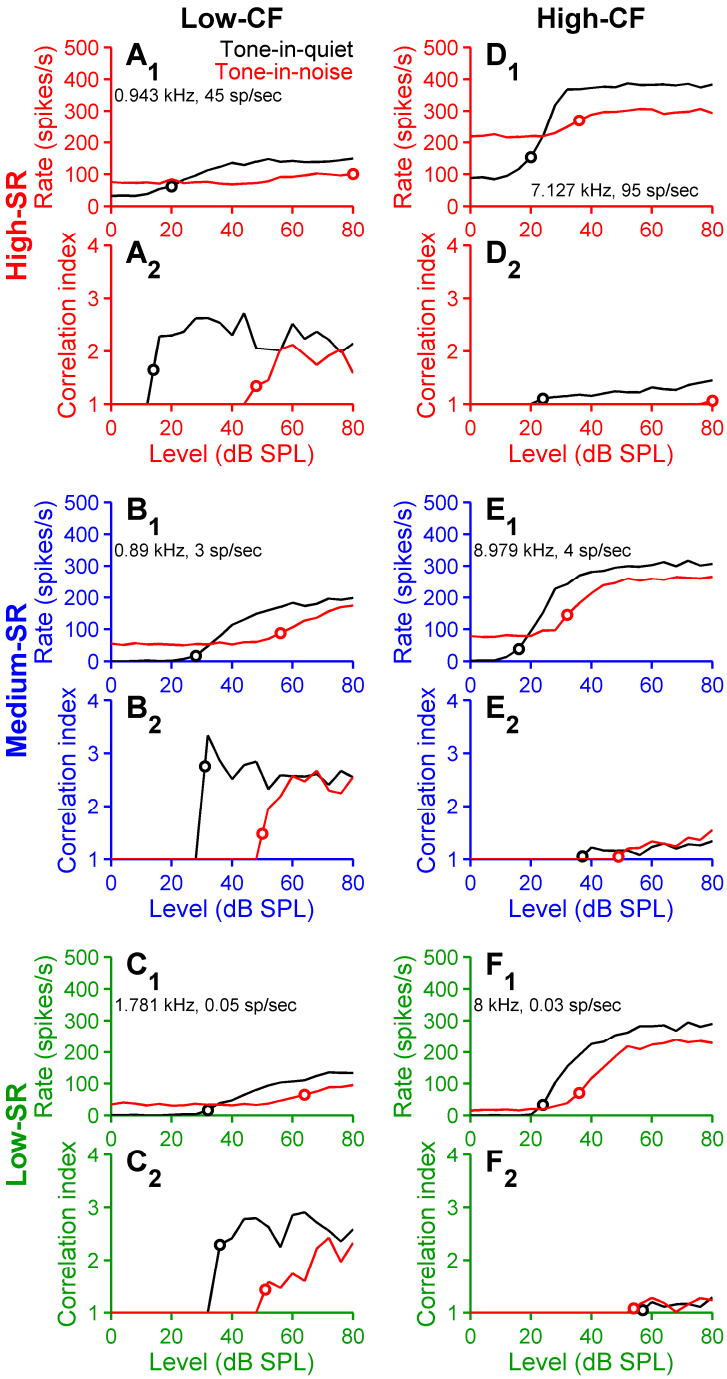

Figure 3. Examples of rate- and CI-intensity functions, in response to tone-in-quiet (black curves) and tone-in-noise (red curves). Rate- (A1, B1, C1, D1, E1, F1) and CI-intensity functions (A2, B2, C2, D2, E2, F2) for six fibers characterized by different CF (low-CF, left column; high-CF, right column) and SR (high-SR, top panels; medium-SR, middle panels; low-SR, bottom panels). On each trace, the open symbols indicate the sound level for which a significant increment of the response was detected using statistical analysis of the neural response as proposed by Huet et al. (2018).

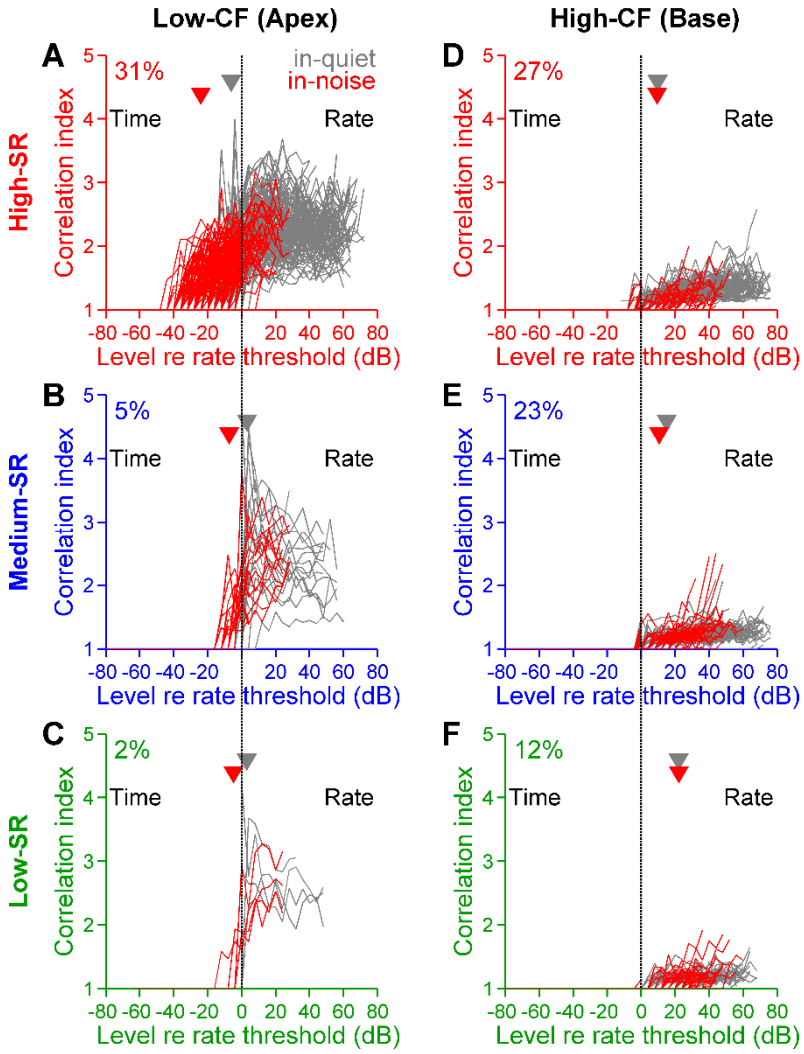

Figure 4: Correlation index as a function of the level relative to rate threshold, in response to tone in quiet (gray traces) and tone in noise (red traces). The entire data set (*n* = 377 ANFs) was classified into 6 pools according to CF (low-CF, CF<2.7 kHz, left column; high-CF, CF>2.7 kHz, right column) and SR (high-SR, SR>18 spikes/sec, top row; medium-SR, 0.5<SR<18 spikes/sec, middle row; low-SR, SR<0.5 spike/sec, bottom row). The percentage of fibers in each group as referred to the entire data set is given. The fibers with a CI-intensity function on the left of the vertical line are able to provide temporal coding without elevating their discharge rate. Triangles in each panel indicate the grand average threshold calculated in quiet (gray) and noisy conditions (red).

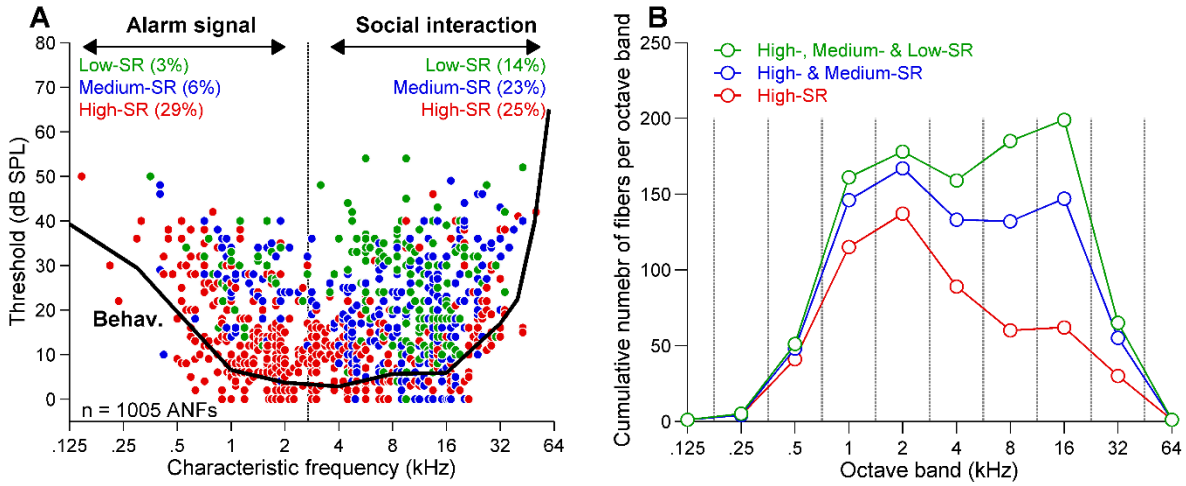

Figure 5: SR-based distribution of ANFs along the tonotopic axis in gerbils. A. Scatter plot of single-fiber thresholds as a function of the fiber characteristic frequency (n = 1005 fibers). The continuous thick line gives the behavioral auditory threshold (Ryan, 1976). The vertical dashed line at 2,7 kHz give the cut-off frequency between the two modes of coding calculated by Huet et al. (2018). The proportion of low-, medium and high below and above 2.7 kHz is given in percent. **B**. Cumulative number of fibers per octave band calculated from data shown in A**.** In A and B, the SR value is represented using a color code with green, blue and red for low- (<0.5 spike/sec), medium-, and high-SR fibers (>18 spikes/sec), respectively.

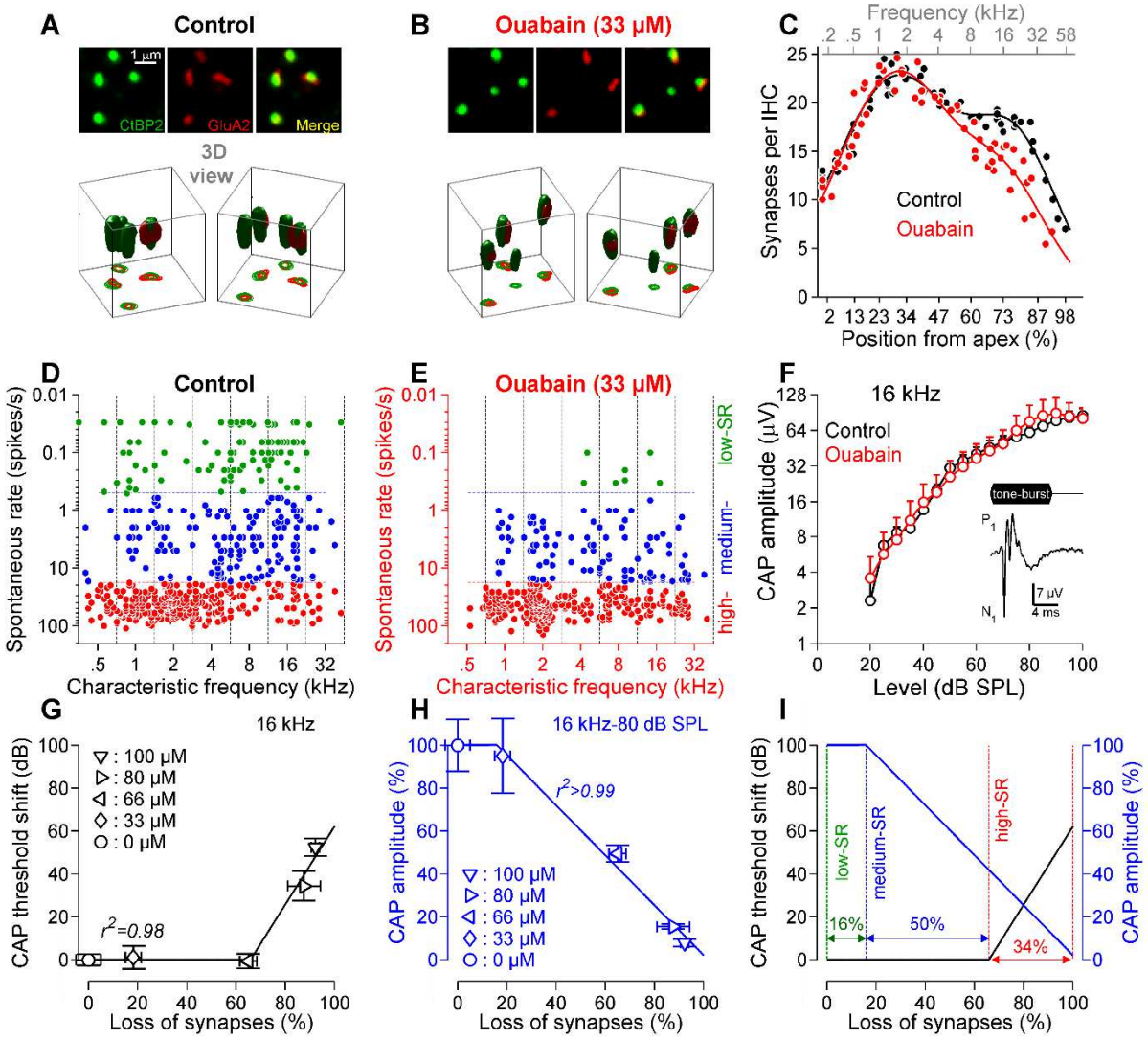

Figure 6. The compound action potential (CAP) of the auditory nerve remains unchanged after the deletion of low-SR fibers. A, B. Confocal microscopy of immunolabeled CtBP2 (green) and GluA2 (red) from the 16-kHz encoding region in artificial perilymph control (A) and ouabain-poisoned cochleae (B). **C**. Synaptic counting in control and ouabain-treated gerbils. Fits are the sum of two Gaussian models ($r^2 \geq 0.88$). **D-E**. Spontaneous rate of ANFs as a function of the characteristic frequency, in control and ouabain-treated animals. SR values are represented using a color map from green (low-SR) to red (high-SR). **F**. CAP amplitude-intensity functions in response to 16 kHz tone burst, in control (black) and ouabain-poisoned cochleae (red). **G, H**. CAP threshold shift (G) and CAP amplitude (H) as a function of the loss of synapses induced by increasing concentration of ouabain (*i.e.* 0, 33, 66, 80, 100 µM). Fits are broken-stick models. **I.** The superposition of fits shown in G and H partitions the fibers in three groups that match with the proportion of low- (green), medium- (blue), and high-SR fibers (red) in the 16 kHz region.

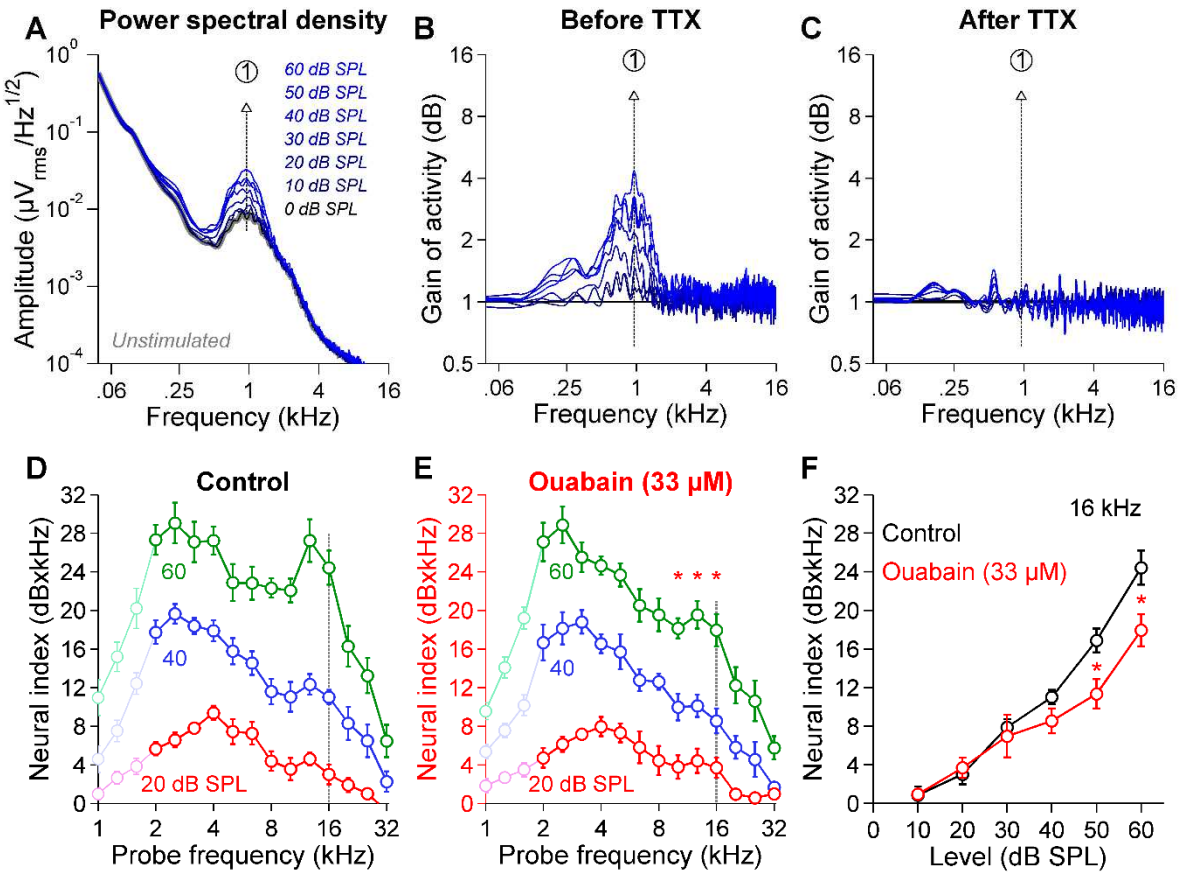

Figure 7. Probing the auditory nerve using round-window mass potentials in control and ouabain-poisoned cochleae. A. Power spectral density (PSD) of the mass potential in the absence of sound stimulation (gray trace) or in response to a third-octave band noise centered on 8 kHz, and different levels varying from 0 to 60 dB SPL, in 10 dB steps. Note the increase of a spectral component at 1 kHz. **B**. Sound-driven activity calculated from panel A, by dividing point-by-point the sound-driven PSDs over the unstimulated PSD. **C**. Same analysis as in panel B, after a 10 µM Tetrodoxin (TTX) application in the round window niche. **D**. The area under the curve in panel B was then measured as a neural index and plotted as a function of the probe frequency, for different levels of stimulation (*i.e.* 20, 40 and 60 dB SPL). **E**. Same analysis as in D, but for a set of gerbils treated with ouabain. Note that for low levels of stimulation (*i.e.* 20 and 40 dB SPL) isolevel functions are unaffected in ouabain-treated gerbils. For a 60 dB SPL stimulation, the amplitude of the isolevel function is reduced in the 16 kHz region (vertical dashed line), *i.e.* in the region populated by low-SR fibers in gerbils. **F**. Neural index *versus* level function at 16 kHz, in control (black) and ouabain-treated gerbils. *, $p<0.05$, Student's t-test.